INTERPARTICLE CONTACT BEHAVIOR AND WAVE PROPAGATION

By Giovanni Cascante[1] and J. Carlos Santamarina[2]

ABSTRACT: The low-strain stiffness and energy dissipation in particulate materials is strongly determined by the behavior of contacts. This paper presents results of a test program designed to study the effect of contact response on the propagation of waves. Wave velocity and attenuation were measured during isotropic loading using a resonant column device at shear strains varying from $\gamma = 10^{-5}$ to $\gamma = 10^{-6}$. Elastic, viscoplastic and brittle contact behaviors were studied with steel spheres, lead shot, and silica-kaolinite pellets. All measured velocity-stress exponents were $b/2 > \approx 1/6$, which is the theoretical value for spherical contacts. High-tolerance steel spheres approximated this value. Contact crushing showed the highest exponent. Theoretical analyses confirmed that several phenomena conduce to a velocity-stress exponent $b/2 = 0.25$: buckling of particle chains and increase in coordination number, elastoplastic behavior, and cone-plane contacts. Load and unload data for viscoplastic lead shot showed that contact deformation is the governing parameter for low-strain stiffness, regardless whether the causing mechanism was elastic deformation, creep, or yield. All measured damping-stress exponents were between $\kappa = -0.45$ for steel and $\kappa = -0.11$ for the brittle pellets, while the theoretical value for frictional Mindlin contacts is $\kappa = -2/3$. Damping showed higher sensitivity than velocity to stress and time.

INTRODUCTION

The deformation of granular materials upon loading involves particle rearrangement and particle deformation. Particle rearrangement and the consequent fabric changes occur at middle and large strains ($\gamma > 10^{-4}$ in general). Fabric changes are affected by surface roughness, degree of frustration of particle rotation, particle size distribution, and interparticle forces. On the other hand, particle deformation is the prevailing deformation mechanism at low strains; it depends mainly on the interparticle contact response and material properties including elastic, viscoplastic, and brittle behaviors. The intervening contact law is not crucial for the constitutive relationships applicable to high strain levels. However, low-strain wave-propagation parameters reflect contact behavior and the state of the assembly.

The exponent b of the power relationship between stiffness and confinement $G \propto \sigma^b$ can be used as an indicator of the type of contact. For example, $b = 1/3$ for spherical contacts between linear-elastic materials, whereas $b = 1/2$ for cone-to-plane contacts. However, such values apply for constant fabric conditions. Goddard (1990) showed that the increase in coordination number among spherical particles due to buckling of particle chains can justify an exponent $b = 1/2$. Moreover, Chang et al. (1991) showed that the shear modulus is proportional to the coordination number to the power 2/3 for a random packing of spheres with Mindlin contacts. In general, prior observations and analyses show that low-strain stiffness depends on coordination number, confining pressure, and contact behavior, including cementation [see Petrakis and Dobry (1987); Acar and El-Tahir (1986)].

The effect of fabric changes on wave-propagation parameters has been previously addressed by the writers (Santamarina and Cascante in press, 1996). The purpose of this study is to assess the effect of different contact behaviors on wave velocity and attenuation. Materials are selected to highlight individual characteristics: elastic Hertzian contacts (steel spheres), viscoplastic deformations and rheological effects (lead shot), and brittle contacts (pellets made of a mixture of silica flour and kaolinite). Finally, a uniform quartz sand is tested for comparison.

PARTICULATE MATERIALS: WAVE PROPAGATION PARAMETERS

Macrowave propagation parameters can be analytically estimated for a particulate medium once the governing contact law, the distribution of contacts, and the distribution of contact forces are known.

Internal Forces

The average normal contact force f_n in an isotropic random assembly of monosized spherical particles can be estimated using the micromechanic formulation by Rothenburg and Bathurst (1989) for a given void ratio e, coordination number C_n, and isotropic confinement σ_0 by

$$f_n = \frac{4\pi(1 + e)R^2\sigma_0}{C_n} \tag{1}$$

In the simplest case of a simple cubic (SC) packing f_n is given by

$$f_n = 4R^2\sigma_0 \tag{2}$$

The average contact stress ($\overline{\sigma_c}$) in a random assembly with Hertzian contacts can be derived from (1) by

$$\overline{\sigma_c} = \left(\frac{1 + e}{C_n}\right)^{1/3} \left[\frac{16G}{3\pi(1 - \nu)}\right]^{2/3} \sigma_0^{1/3} \tag{3}$$

Relationships (1) and (3) can be simplified by replacing empirical or theoretical equations that relate coordination number and void ratio. For example (Smith et al. 1929)

$$C_n = 26.486 - 10.726(1 + e) \tag{4}$$

Limiting the force at contacts [(1)] to the force in a SC array [(2)], leads to the following upper bound expression for the coordination number:

$$C_n \geq \pi(1 + e) \tag{5}$$

which is in agreement with prior experimental results for particulate materials with $e < 0.9$ (Smith et al. 1929; Field 1963).

Elastic Contact

The normal stiffness k_n of two elastic spheres in contact can be computed from the Hertzian relationship between the normal contact force f_n and the center-to-center displacement d by

[1]Post Doctoral Fellow, University of Waterloo, Waterloo, Canada.
[2]Assoc. Prof., Dept. of Civ. and Envir. Engrg., Georgia Institute of Technology, Atlanta, GA 30332; formerly at University of Waterloo, Canada.

Note. Discussion open until March 1, 1997. To extend the closing date one month, a written request must be filed with the ASCE Manager of Journals. The manuscript for this paper was submitted for review and possible publication on November 8, 1995. This paper is part of the ***Journal of Geotechnical Engineering***, Vol. 122, No. 10, October, 1996. ISSN 0733-9410/96/0010-0831–0839/$4.00 + $.50 per page. Paper No. 12040.

$$k_n = \frac{df_n}{d\delta} = 3\left[\frac{G_m}{3(1-\nu)}\right]^{2/3} f_n^{1/3} \tag{6}$$

where G_m and n = the shear modulus and the Poisson's ratio of the material, respectively. This relationship can be extended to determine the tangential normal stiffness E_T of a SC packing with Hertzian contacts by [e.g., Richart et al. (1970)]

$$E_T = \frac{3}{2}\left[\frac{2G_m}{3(1-\nu)}\right]^{2/3} \sigma_0^{1/3} \tag{7}$$

where σ_0 = confinement. Hertzian relationships can also be manipulated to determine an expression for E_T as a function of the axial strain ε_z by

$$E_T = \frac{G_m}{(1-\nu)} \varepsilon_z^{1/2} \tag{8}$$

The variation of stiffness with confinement to the power 1/3 shown in (6) and (7) applies to other regular packings (Duffy and Mindlin 1957; Deresiewicz 1974; Petrakis and Dobry 1987). Tangential forces have an important effect on the stiffness of particulate materials; Duffy and Mindlin (1957) showed for a face-centered cubic (FCC) packing that the ratio of compressional stiffness E_M, when the tangential forces are considered, to the stiffness E_H, when tangential forces are neglected, is

$$\frac{E_M}{E_H} = \frac{3(8-7\nu)}{(8-5\nu)} \tag{9}$$

When $\nu = 0.20$, the ratio becomes $E_M/E_E = 2.8$.

The variation of stiffness with normal force for a conical contact was studied by Goddard (1990); in this case the normal stiffness is given by

$$k_n = \frac{df_n}{d\delta} = \left[\frac{8G_m}{\pi(1-\nu)\alpha}\right]^{1/2} f_n^{1/2} \tag{10}$$

where α = the angle between the cone and the normal plane. The exponent of the normal contact force in (10) is 1/2 in comparison with 1/3 for the Hertzian contact [(6)]. Goddard (1990) suggested that conical contacts could explain the common observation that the stiffness on dry sands varies with isotropic confinement with exponents close to 1/2, instead of the 1/3 predicted for Hertzian contacts.

Theoretical expressions for attenuation under different contact laws are scarce. Considering frictional attenuation, the FCC and SC regular packings of spheres present a decrease in damping D with confinement σ_0 at low shear strains given by

$$D = C\sigma_0^{\kappa} \tag{11}$$

where C = a constant. The exponent for Mindlin contacts is $\kappa = -2/3$ (Duffy and Mindlin 1957; Petrakis and Dobry 1987). However, experimental evidence shows that other loss mechanisms are involved at low strains, $\gamma < 10^{-5}$ (Santamarina and Cascante, 1996).

Viscoplastic Contact

Lee and Radok (1960) developed a contact solution for a viscoplastic material based on Hertz's solution by exchanging elastic constants with linear operators. They found that the viscoplastic pressure distribution at the contact is close to the elastic solution when the selected time t is shorter than the relaxation time ($t < t_0$). For times longer than t_0, the pressure distribution shows a dimple at the center of the contact due to the effect of preindentation; therefore, the maximum stress occurs close to the edges of the contact and not at the center as in the elastic case.

When the parameter of interest is the tangential global stiffness E_T, the stress distribution within a particle is not as important as the stiffness of the deformed particle. Therefore, it appears that the Hertzian relation E_T versus ε[(8)] can be generalized to more complex material behaviors at constant fabric. This presumes that the small strain wave excites an elasto-viscoplastic material as an elastic medium, and that it is of little importance whether the current deformed geometry was reached by elastic, viscous, or plastic deformations.

Considering the pressure distribution at the contact as a constant stress acting on a circular area (this is in agreement with the distribution for $t > t_0$), the radius of the contact area in SC arrays under isotropic stress σ_0 is

$$r = \left[\frac{4}{\pi}\frac{\sigma_0}{\sigma_y}\right]^{1/2} R \tag{12}$$

where R = the radius of spherical particles; and σ_y = yield stress of the material. By trigonometry, the strain in the array ε can be related to the radius r of the contact area by

$$\varepsilon = \left(\frac{r}{R}\right)^2 \tag{13}$$

Substituting (12) and (13) into the expression for tangent modulus for a SC packing derived from Hertz's theory [(8)], an approximation for the tangential normal stiffness of an a elastoplastic material can be obtained

$$E_T = \frac{2G_m}{\pi^{1/2}(1-\nu)}\left[\frac{\sigma_0}{\sigma_y}\right]^{1/2} \tag{14}$$

Therefore, the stiffness of the assembly varies with confinement to the exponent $b = 1/2$. The same conclusion was reached following the solution proposed by Lee and Radok (1960).

Brittle Contact

The authors are not aware of any solution for low strain parameters in particulate materials with brittle contacts. Crushing of contacts should produce a faster variation in stiffness than elastic deformations. Then, a higher exponent b can be expected for the stress range that causes crushing.

Empirical Relations—Real Particulate Materials

Empirical expressions for G_{max} have been proposed for soils under isotropic loading σ_0. In general, these equations are of the following form:

$$G_{max} = Af(e)\sigma_0^b \tag{15}$$

Given that $V_s = \sqrt{(G/\rho)}$, then

$$V_s = a\sigma_0^{b/2} \tag{16}$$

where a and b = constants; and $f(e)$ = a function of void ratio [e.g., Hardin and Black (1966); Hardin and Drnevich (1972); Stokoe et al. (1985); Saxena et al. (1988)]. Empirical corrections for void ratio are similar; the one proposed by Hardin and Drnevich (1972) is

$$f(e) = \frac{(2.97-e)^2}{1+e} \tag{17}$$

The empirical equation, (15), after substituting $f(e)$ by (17), is remarkably similar to micromechanics-based equations for random packings of spheres (Chang et al. 1991). Equations for E_T can be rewritten in terms of G_{max} using the standard relation between E and G for isotropic materials.

The variation of damping in geomaterials due to changes in confinement and excitation level has been modeled with hy-

perbolic models (Ishihara 1986). These models adequately characterize frictional losses. Santamarina and Cascante, in press, (1996) proposed a modified hyperbolic model; it includes a minimum damping at low strain levels $\gamma < \approx 10^{-5}$, which depends only on confinement.

EXPERIMENTAL STUDIES

The standard resonant column device (SBEL D1128) and test procedure were modified to decrease the shear strain imposed during testing. Band-limited random noise was used as excitation. Device modifications and test procedures were described in Cascante and Santamarina (in press, 1996).

Tested materials were selected to experimentally study the effect of contact behavior on wave-propagation parameters. These studies were conducted on random packings of uniform size, quasispherical particles, including steel spheres, lead shot, silica-kaolinite pellets, and round hard-grain sand. Table 1 summarizes the main characteristics of the selected particulate materials.

Samples were prepared by the dry pluviation technique from a constant falling height. Once the upper platen was set in place, vacuum was applied to hold the sample and the split mold was removed. Then, connections for the driving plate, LVDT, and accelerometer were made, and the chamber was assembled. Sample vacuum was gradually released while increasing the cell pressure, until an effective confinement of σ_0 = 35 kPa was reached. Isotropic loading (IL) was applied to all samples tested in this study, increasing the confining pressure.

The size of steel spheres, lead shot, and pellets allowed significant membrane penetration for pressures higher than 300 kPa. Membrane rupture at the interface with platens was prevented with a thin plastic tape around the perimeter of top and bottom caps. The height of samples was $H \approx 13$ cm, hence $\lambda \gg D_{50}$ for the first resonant mode, and the wave traversed samples as a continuum.

Elastic Contact Behavior (Steel Spheres)

High-strength steel was selected to study the effect of isotropic confinement on wave-propagation velocity and attenuation in a random packing of elastic monosized spheres. The main characteristics of the chrome steel spheres are summarized in Table 1. The initial void ratio was $e \approx 0.60$, which is close to the general value for a random assembly of smooth monosized spheres [$e = 0.57$ (Scott et al. 1964)]. High-precision steel spheres have accurate dimensions and smooth surfaces; thus, simple micromechanical models with Hertz and Mindlin theories can be attempted to analyze the results.

Steel spheres were cleaned with acetone and detergent before sample preparation in order to avoid the effect of adsorbed layers of grease [see also Duffy and Mindlin (1957)]. The coupling between the sample and platens was enhanced by adding gypsum on each end of the sample.

Test Results

The stress-strain behavior during loading and unloading is presented in Fig. 1(a). The maximum vertical strain was $\varepsilon_z = 0.025\%$; the small residual strain $\varepsilon_z = 0.005\%$ indicates limited fabric changes. The axial strain ε_z for a SC array can be estimated in terms of the confinement σ_0 as

$$\varepsilon_z = \left[\frac{3(1-\nu)}{2G}\sigma_0\right]^{2/3} \tag{18}$$

For FCC, the expression for incremental strain given by Duffy and Mindlin (1957) can be integrated to determine the isotropic strain ε_0 by (Richart et al. 1970)

TABLE 1. Characteristics of Tested Materials

Granular material (1)	Unit weight (kN/m³) (2)	Initial void ratio (3)	Final void ratio (4)	Particle size (mm) (5)	Approximate number of particles (6)
Steel spheres	78.1	0.60	0.60	3.18 ± 0.00254	1.9×10^4
Lead shot	113.6	0.69	0.64	1.0–1.5	2.6×10^3
SF-K pellets	18.5[a]	1.22[b]	0.78[b]	1.19–3.35	1.9×10^4
Uniform sand	26.5	0.60	0.59	0.20–0.45	7.4×10^6

[a]Internal void ratio of pellets $e_p = 0.43$.
[b]Global void ratio = void ratio of pellets + void ratio packing.

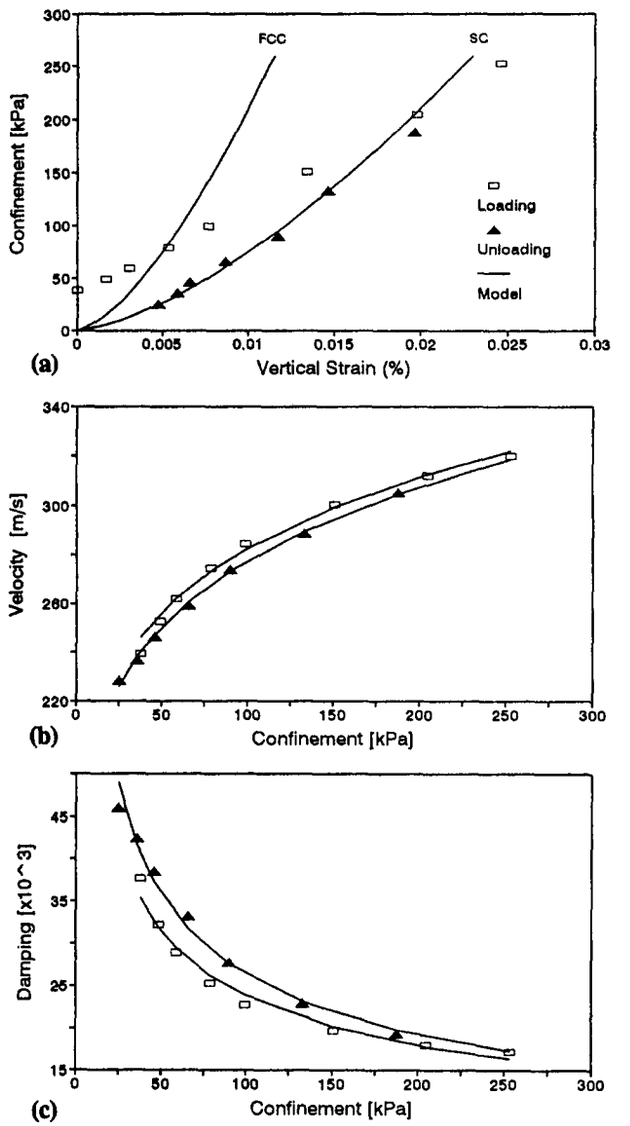

FIG. 1. Elastic Contact Behavior; Steel Spheres Subjected to Isotropic Loading: (a) Stress-Strain Response and Predictions Based on Simple Cubic (SC) and Face-Centered Cubic (FCC) Packings; (b) Velocity versus Confinement; (c) Damping versus Confinement

$$\varepsilon_0 = \frac{1}{2}\left[\frac{3(1-\nu)}{2G}\sigma_0\right]^{2/3} \tag{19}$$

Therefore, the FCC array is twice stiffer than the SC packing because of the higher coordination number (FCC-C_n = 12; and SC-C_n = 6), lower void ratio, and the additional mobilization of Mindlin stiffness at contacts. Eqs. (18) and (19) are also plotted in Fig. 1(a), using the elastic properties of steel spheres. The SC packing model predicts a stress-strain curve

remarkably similar to values measured during unloading, despite the simplicity of the model. For a random packing with $e = 0.6$, the coordination number is $C_n \approx 9$ (4). However, the measured stiffness is lower than or equal to the stiffness predicted for a SC with $C_n = 6$. This is a clear example of the effect of fabric: regular packings tend to "lock" manifesting high stiffness.

The variation of shear-wave velocity with confinement is shown in Fig. 1(b). This trend follows the standard power relationship (16). The measured value of the velocity-stress exponent is $b/2 \approx 0.15$, which is slightly lower than the theoretical value $b/2 = 1/6 = 0.167$ [Fig. 1(b)]. Loading and unloading paths are similar; however, velocity is consistently smaller during unloading than during loading, indicating a reduction in low-strain shear stiffness ($\gamma < 10^{-5}$), contrary to the trend observed for midstrain stiffness [Fig. 1(a)]. This decrease in stiffness may reflect a reduction of contact forces, since the coordination number is expected to increase during loading [(1), (4), and (6)]; even though shear stiffness is proportional to coordination number for a given confinement and void ratio (Chang et al. 1991).

Another hypothesis is the reduction in contact stiffness due to contact deterioration during loading. The minimum isotropic confinement necessary to produce an average contact stress equal to the yield stress, was estimated with (3) and (4). For the elastic parameters of the steel spheres and a representative void ratio $e = 0.6$, the computed value is $\sigma_{avg} = 196$ kPa. On the other hand, the minimum value of confinement required to initiate yielding at the contact is $\sigma_{min} = 58$ kPa. These values are not absolute low-bounds, since they were computed assuming a uniform distribution of contacts and forces. Locally, this is not the case due to random packing and tolerance in the geometry of real steel spheres.

The tolerance in the size of the steel spheres ($\Delta\phi = 0.00254$ mm) exceeds the maximum displacement between two particles, $\delta = 2R\varepsilon_z$, for all levels of confinement. Assuming that the random packing is made of a combination of regular packing cells, this tolerance in size implies that some contacts are never formed, even at the highest pressure used in this study. Duffy and Mindlin (1957) tested a granular bar made of steel spheres of the same diameter but with two tolerances ($\Delta\phi$ = 0.000254 mm and 0.00127 mm) arranged in FCC packing, under confining pressures between 10 kPa and 100 kPa. They found that the exponent $b/2$ was close to the theoretical value ($b = 1/6$) for the high-precision spheres; however, it was higher than 1/6 for the lower-precision spheres. Higher precision spheres also led to higher velocities, due to the higher number of contacts.

The reduction in damping with confining pressure is shown in Fig. 1(c). In agreement with (11), damping shows a dependence on confining pressure, with $\kappa = -0.41$ for loading and -0.45 for unloading. The increase in damping during unloading is consistent with the observed decrease of shear-wave velocity, since an increase in stiffness is usually related to a reduction in attenuation, for example, hyperbolic models. Duffy and Mindlin (1957) measured $\kappa = -1/3$ in the granular bar with FCC packing. However, their analytical solution based on the integration of the hysteresis loop predicted an exponent $\kappa = -2/3$. Duffy and Mindlin (1957) also reported that energy dissipation doubled when steel spheres were just cleaned with acetone in comparison with spheres well cleaned with successive baths of carbon tetrachloride, toluol, and acetone. Therefore, surface layers play an important role in energy-loss mechanisms.

Visco-Plastic Contact Behavior (Lead Shot)

Lead shot was tested to study the effect of rheological contact changes on wave propagation. The characteristics of lead shot are summarized in Table 1. Lead shot was not cleaned before sample preparation. A thermocouple was mounted at the bottom of the sample to monitor internal temperature during testing. The average temperature was 21 ± 1°C. Wave parameters were determined at preselected isotropic confining pressures: 72, 141, 262, and 576 kPa. Each pressure level was maintained for a minimum of 50 h. Measurements were also conducted during unloading at 502, 408, 301, 200, 101, and 51 kPa, keeping the load constant for 3 h at each stage.

Test Results

The maximum strain reached upon loading was $\varepsilon_z \approx 1.0\%$ [Fig. 2(a)]. Unloading showed very small strains and was probably accompanied by limited contact and fabric changes [Fig. 2(a)]. Contacts were plastically deformed and the elastic recovery of lead particles was small ($\Delta\varepsilon_z \approx 0.05\%$). The σ-ε trend was quasi-linear for loading and unloading, indicating a constant midstrain stiffness. The void ratio decreased from $e = 0.688$ to $e = 0.641$. Volumetric strains were estimated from

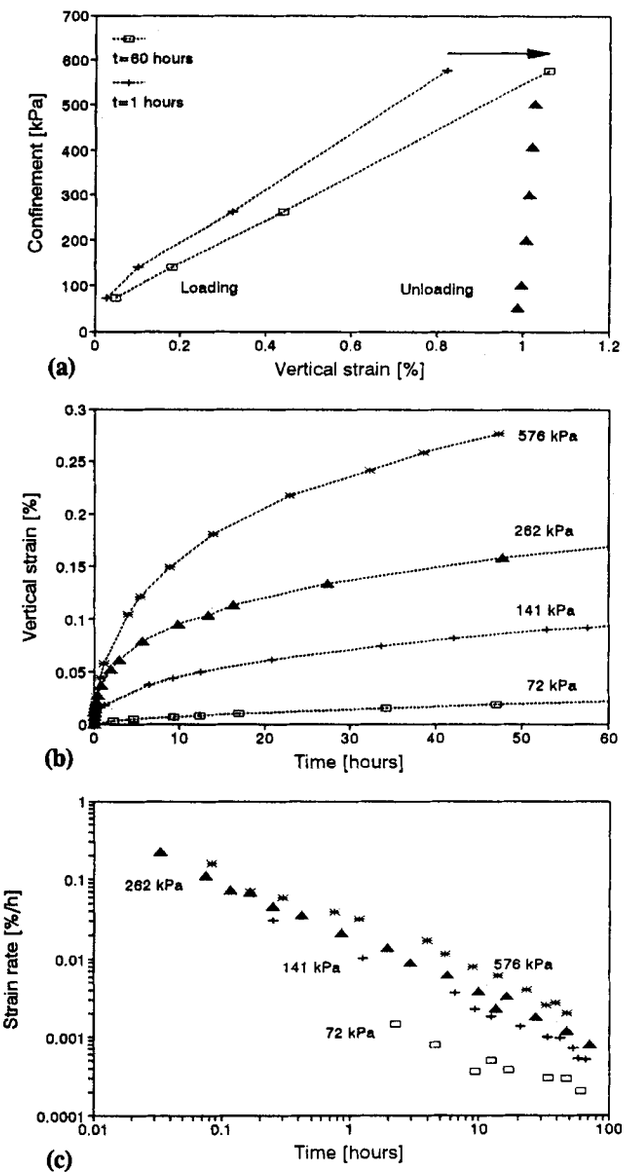

FIG. 2. Visco-Plastic Contact Behavior; Lead Shot Subjected to Isotropic Loading: (a) Stress-Strain Curve: $t = 1$ h, $t = 60$ h, and Unloading; (b) Vertical Strain versus Time: Confinement $\sigma_0 = 72$, 141, 262, and 576 kPa; (c) Strain Rate versus Time: Confinement $\sigma_0 = 72$, 141, 262, and 576 kPa

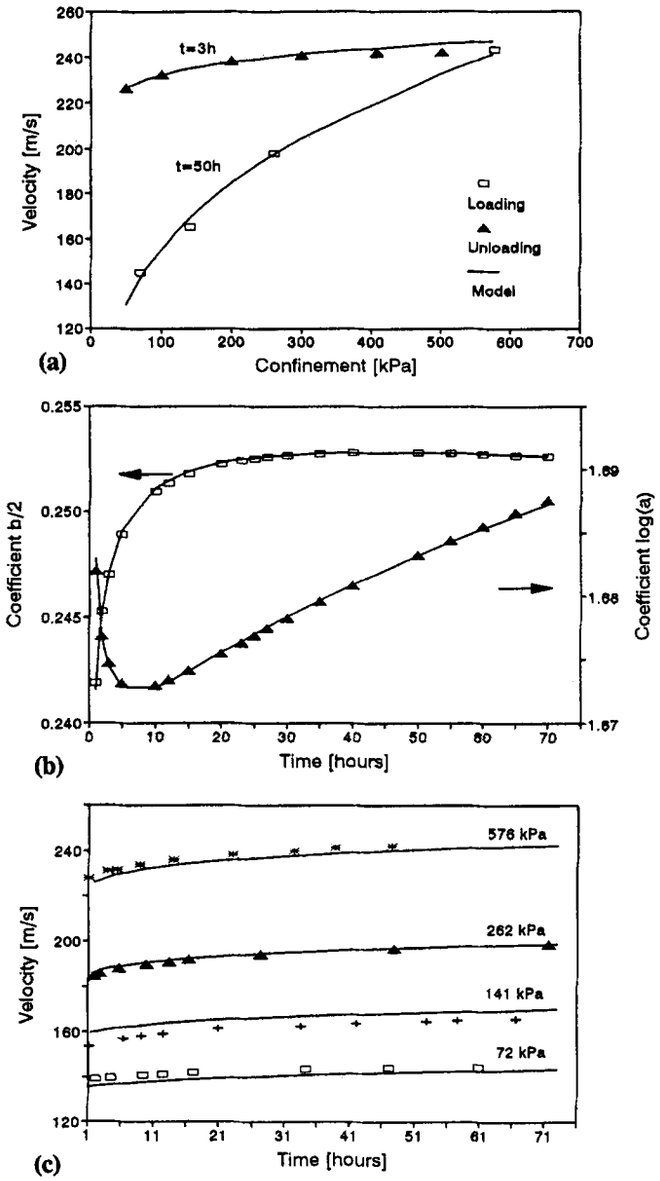

FIG. 3. Visco-Plastic Contact Behavior; Lead Shot Subjected to Isotropic Loading: (a) Velocity versus Confinement: Loading (t = 50 h) and Unloading (t = 3 h); (b) Coefficients $b/2$ and log(a) as Function of Time; (c) Velocity versus Time: Confinement σ_0 = 72, 141, 262, and 576 kPa

the measured vertical strain $\varepsilon_{vol} = 3\varepsilon_z$. This procedure was verified by measuring the final volume of the sample; results differed in less than 10%.

The change in vertical strain with time is presented in Fig. 2(b) (strain is zeroed at each load increment). The corresponding strain rates are plotted in Fig. 2(c). Creep follows an exponential law, as in diffusion and dislocation mechanisms (Feda 1992). The time window was not sufficient to observe steady-state creep for all confinements [Fig. 2(c)]. The Weertman constitutive model is most often used to relate the steady-state creep rate $\dot{\varepsilon}_{ss}$ to the stress difference σ and the absolute temperature T by

$$\dot{\varepsilon}_{ss} = A\sigma^{n_0} e^{-Q/R_0 T} \tag{20}$$

where A and n = constants; Q = creep activation energy; and R = the gas constant. For particulate materials, the following empirical equation has been proposed for the strain rate $\dot{\varepsilon}$ (Singh and Mitchell 1968):

$$\dot{\varepsilon} = k\left[\frac{\sigma}{\sigma_{re}}\right]^m \left[\frac{t_{re}}{t}\right]^n \tag{21}$$

where k, m, and n = constants that depend on the material; and σ_{re} and t_{re} = reference stress and time, respectively. The axial strain can be obtained by integrating (21). Finally, stiffness can be computed by generalizing the Hertzian relation [(8)], leading to a general expression for velocity as a function of time t and confinement σ_0

$$V(\sigma_0, t) = a\left[\frac{\sigma_0}{\sigma_{re}}\right]^{b/2} \left[\frac{t_{re}}{t}\right]^{n_1} \tag{22}$$

where a, $b/2$, and n_1 = parameters related to the constants in (8) and (21). The exponent n_1 reflects the rate of contact creep changes, and $b/2$ the common dependence of velocity on confinement [(16)].

Velocity-stress data are plotted in Fig. 3(a) and show that velocity follows the standard power law upon loading, yet V_s remains almost constant during unloading, showing strong preloading effects, i.e., permanent deformation of contacts. Velocity-stress trends were fitted with the power equation, (16), for velocity values at different times. Best-fit $b(t)/2$ and $a(t)$ parameters are plotted versus time in Fig. 3(b), together with a best-fit parabolic trend. The increase in $b/2$ with time indicates that creep effects are accentuated at high confinement. Long-term changes in $a(t)$ also show an increase with time. On average, $b/2 \approx 0.25$ as predicted by (14). The average increase in velocity due to creep was $\Delta V \approx 6\%$ in 50 h [Fig. 3(c)], which would correspond to a 30% increase in confinement.

The measured variation of wave velocity with time and confinement $V_s(\sigma, t)$ are shown in Fig. 3(c). These data were fitted with (22), fixing $b/2 = 0.25$ and $\log(a) = 1.68$, rendering the exponent $n_1 = 0.31$. Trends shown in Fig. 3(c) correspond to (16), and the parabolic relations for $b(t)/2$ and $a(t)$ shown in Fig. 3(b).

Damping decreased exponentially with confining pressure

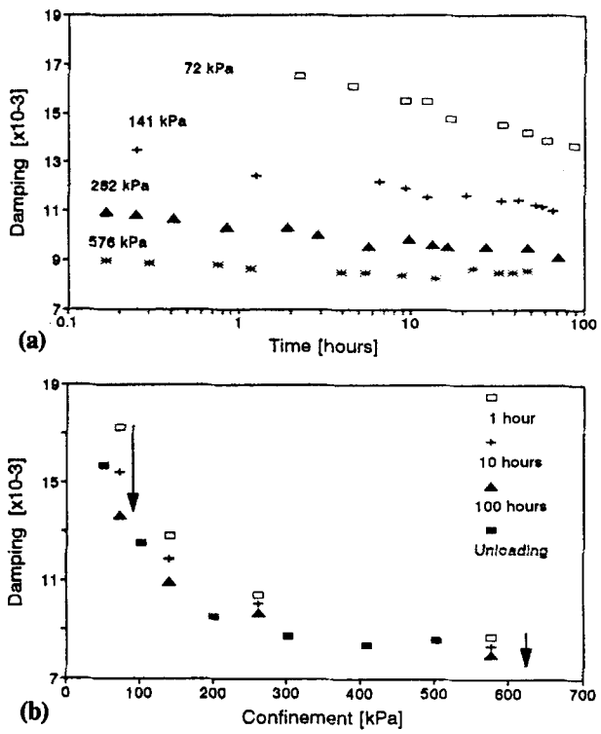

FIG. 4. Visco-Plastic Contact Behavior; Lead Shot Subjected to Isotropic Loading: (a) Damping versus Time: Confinement σ_0 = 72, 141, 262, and 576 kPa; (b) Damping versus Confinement: Loading (t = 1, 10, and 100 h) and Unloading

and linearly with the logarithm of time [Figs. 4(a and b)]. Again, the back-calculated exponent $\kappa = -1/3$ was smaller the than theoretical prediction for hysteretic Mindlin contacts ($\kappa = -2/3$). The relative change in damping due to rheological effects was 4% at low confinement and 20% at high confinement within a 50 h period. These changes would correspond to changes in confinement of 13% and 77%, respectively. Clearly, attenuation is more sensitive than shear-wave velocity to time effects as confinement increases.

Figs. 5(a and b) show velocity and damping data replotted versus vertical strain, respectively. Even though, time and pressure are varying, the trend in velocity follows a clear single trend. Thus, it can be concluded that the deformed geometry of the contact is the governing parameter on wave velocity. As it was earlier hypothesized for constant fabric condition, the experimental evidence shows that the increase in low-strain stiffness is the same whether contact area increases due to confinement or due to creep. The fitting exponent for the V_s versus ε data is 0.29 [Fig. 5(a)], which approaches the theoretical value 1/4 from (8). A general exponential variation of damping with vertical strain is also suggested by Fig. 5(b); however, there are sudden increments in damping immediately after the application of each load increment. It is hypothesized that syntherisation and self-healing of lead takes place at contacts during creep, and that these contact-enhancing effects are reversed when new loading is applied. Velocity remains unaffected by these processes and reflects only the improvement in stiffness by the flattening of contacts.

Velocity changes during unloading were small, confirming the importance of contact geometry over contact forces on low-strain stiffness. Damping increased during unloading, reaching almost original values. Hysteretic frictional behavior depends on normal force and is independent on contact area (Amonton's laws).

Brittle Contact Behavior (Silica-Kaolinite Pellets)

A mixture of 71% silica-flour and 29% kaolinite was used to prepare spherical brittle pellets of average radius $R = 1.3$ mm. Pellets were made in a rotating cylindrical container, with longitudinal axis inclined 20° from the horizontal. The cylinder rotated at 50 RPM, for a total of 1,200 revolutions. The water content required for pelletization was 16%. The surface roughness of pellets reflects the presence of silica flour, and scattered, 10–50 μm sized conglomerates can be found attached to the surface. Pellets were air dried ($w = 0.2\%$) and sieved before testing. The initial grain size distribution is shown in Fig. (6).

The maximum carrying force of a pellet was measured by increasing the force applied on a disk resting onto three pellets until failure. The force per pellet was normalized by the equivalent area of a pellet in SC packing to obtain an estimate of the crashing capacity $q_u = \text{load}/4R^2$. The average ultimate capacity was $q_u = 145$ kPa, with a standard deviation of 50 kPa.

Test Results

Axial deformations were significant during isotropic loading, reaching $\varepsilon_z \approx 9.0\%$ at $\sigma_0 = 500$ kPa; most of the deformation was permanent [Fig. 7(a)]. The small-strain stiffness of the specimen, $\Delta\sigma_z/\Delta\varepsilon_z$, changes rapidly at low strains ($\varepsilon_z < 0.04\%$), remains constant at middle strains ($0.04 < \varepsilon_z < 5.0\%$), and increases for $\varepsilon_z > 5\%$. Unloading shows strong preloading effects. The hardening effect at large strains was caused by densification of the sample, when crushed grains accommodate within void spaces increasing coordination and decreasing stress concentration on intact grains. When the test was finished, the sample did not fail at zero confinement. The global initial and final void ratios of the sample were $e_0 = 1.22$ and

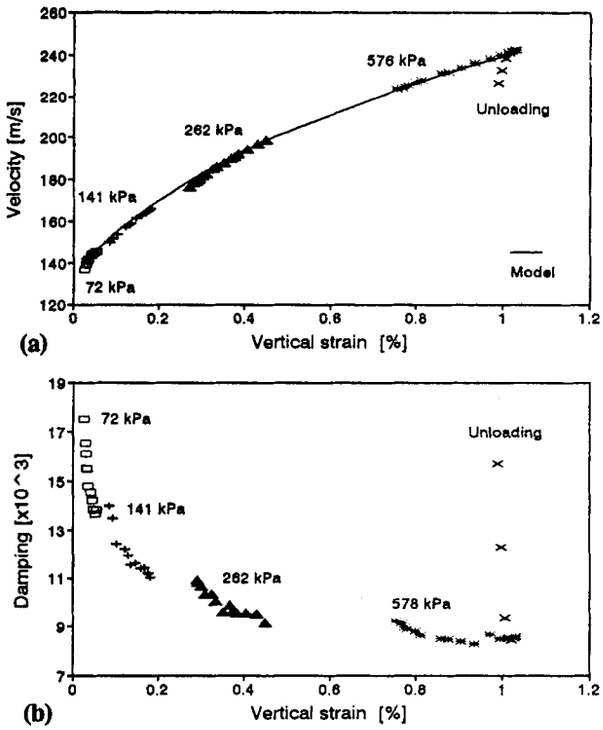

FIG. 5. Visco-Plastic Contact Behavior; Lead Shot Subjected to Isotropic Loading: (a) Velocity versus Vertical Strain: Loading (σ_0 = 72, 141, 262, and 576 kPa) and Unloading; (b) Damping versus Vertical Strain: Loading (σ_0 = 72, 141, 262, and 576 kPa) and Unloading

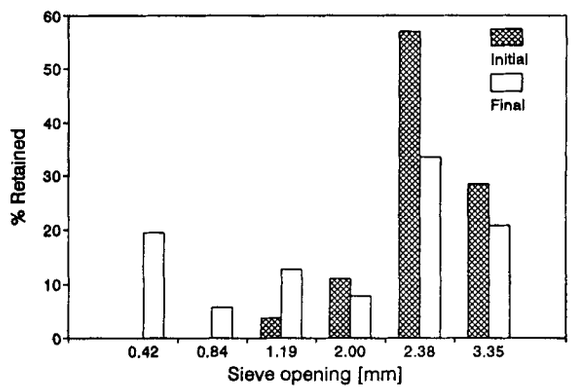

FIG. 6. Silica Flour and Kaolinite SF-K Pellets; Initial and Final Grain Size Distributions

$e_f = 0.77$, respectively. The internal void ratio of pellets was $e_p = 0.43$.

The crushing of grains was monitored with the accelerometer mounted on the driving plate of the resonant column. Most microtremors occurred between $\varepsilon_z \approx 2.0\%$ and $\varepsilon_z \approx 5.0\%$. The corresponding confining pressures agree well with the measured crashing capacity of pellets ($q_u = 145 \pm 50$ kPa).

Shear-wave velocity is plotted versus stress in Fig. 7(b). The exponent $b/2$ for the velocity-stress relationship is $b/2 = 0.33$ for $\sigma_0 < 160$ kPa, where crushing occurred, whereas $b/2 = 0.25$ for confinements $\sigma_0 > 160$ kPa. No significant time dependence of velocity was observed. During unloading [Fig. 7(b)] the exponent was $b/2 = 0.15$, suggesting limited fabric changes.

Damping presents more variability to confinement than shear-wave velocity [Fig. 7(c)], decaying with confinement following (11), with exponents $\kappa = -0.15$ and -0.11 for loading and unloading, respectively. Damping increases immediately after loading, showing sensitivity to the rate of defor-

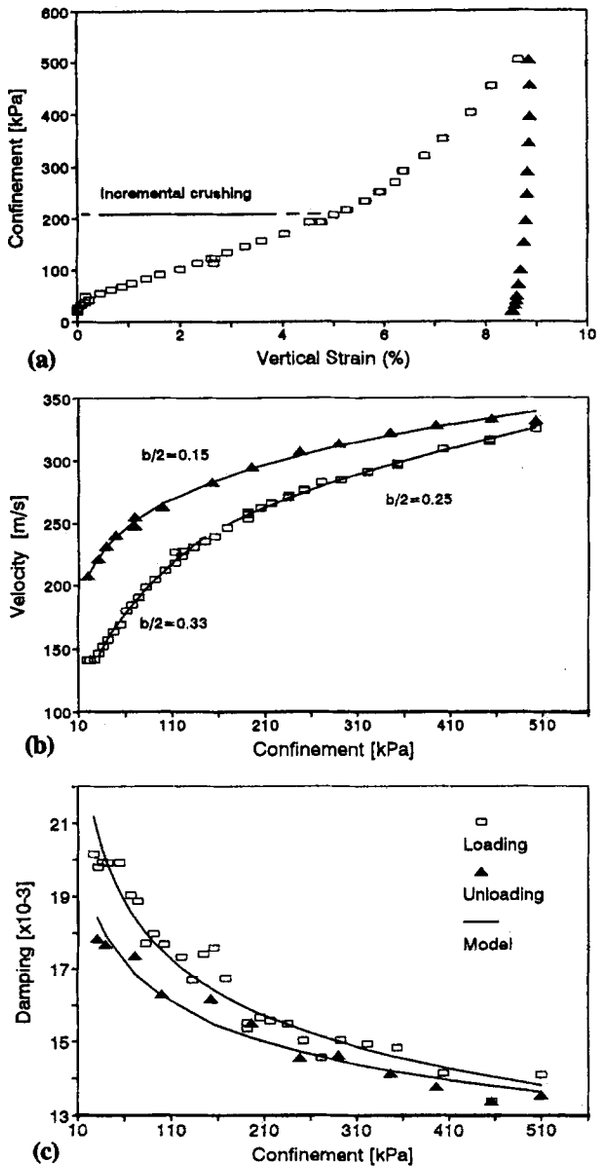

FIG. 7. Brittle Contact Behavior; SF-K Pellets Subjected to Isotropic Loading: (a) Stress-Strain Curve; (b) Velocity versus Confinement; (c) Damping versus Confinement

mation of contacts, as in the case of lead shot; data shown in Fig. 7(c) correspond to damping values measured after deformation stabilized and when microtremors ceased (approximately 15 min after loading).

Real-Soil Contact Behavior (Hard-Grain, Uniform Sand)

Finally, results for a uniform, hard-grain sand are presented for comparison (e = 0.60; Dr = 76%). Its macroresponse is the result of elastic, viscoplastic, and brittle contact behavior. Barco sand 32 has D_{50} = 0.44 mm; e_{max} = 0.73; e_{min} = 0.56; C_u = 1.5; C_c = 0.96; and SiO_2 content 99.6%; additional characteristics are given in Table 1.

Test Results

The stress-strain curve manifests a minor concavity toward the pressure axis as it is expected in isotropic testing of particulate materials [Fig. 8(a)]. The maximum strain at σ_0 = 700 kPa was ε_z = 0.18%. The residual strain upon unloading was ε_r = 0.03%.

The shear modulus (G_{qs}) was computed during isotropic loading and unloading taking into consideration the strain between loading stages $\Delta\varepsilon_z$ (ν = 0.2) by

$$G_{qs} = \frac{(1 - 2\nu)}{2(1 + \nu)} \frac{\Delta\sigma_0}{\Delta\varepsilon_z} \tag{23}$$

Strain changes $\Delta\varepsilon_z$ varied between 10^{-3}% and 10^{-2}%. Values of G_{max} were computed from wave-velocity data obtained at each stage, $\gamma \approx 10^{-5}$. Results are presented in Fig. 8(b). The shear modulus G_{max} shows a small decrease during unloading, which can not be justified by the increase in density during loading; therefore, permanent contact changes and some effect of the limited fabric changes must be considered. The quasi-static midstrain modulus G_{qs} increased significantly during unloading, showing clear sensitivity to preloading effects.

Low-strain shear-wave velocity ($\gamma < 10^{-5}$) is plotted versus confinement in Fig. 9(a). The back-calculated exponent $b/2$ = 0.25 is the same for loading and unloading, and agrees with published data for dry sands [e.g., Hardin and Richart (1963)].

Knowing the unconfined strength of quartz q_u, (3) and (4) can be used to compute the required confining pressure to produce a contact average stress of $\sigma_c = 3.15*q_u$, which corresponds to the bearing capacity of a circular footing on a rigid-plastic half-space. For quartz ($q_u = 3.2*10^5$ kPa; ν = 0.15) and for a representative void ratio e = 0.6, the minimum confining pressure required to generate an average contact stress of $\sigma_c = 3.15*q_u$ is σ_0 = 1,025 kPa. Thus, there is low probability of contact failure within the range of pressure used in these tests. In the absence of flattened contacts by yield or failure, the value of $b/2$ = 0.25 indicates either fabric changes or the prevalent effect of angular contacts, or both.

Damping values measured 10 min after the application of each confinement are shown in Fig. 9(b) together with the corresponding power fitting. Damping is almost constant for confinement σ_0 > 500 kPa. The exponent of the fitting curve is $\kappa = -0.20$ for loading and unloading.

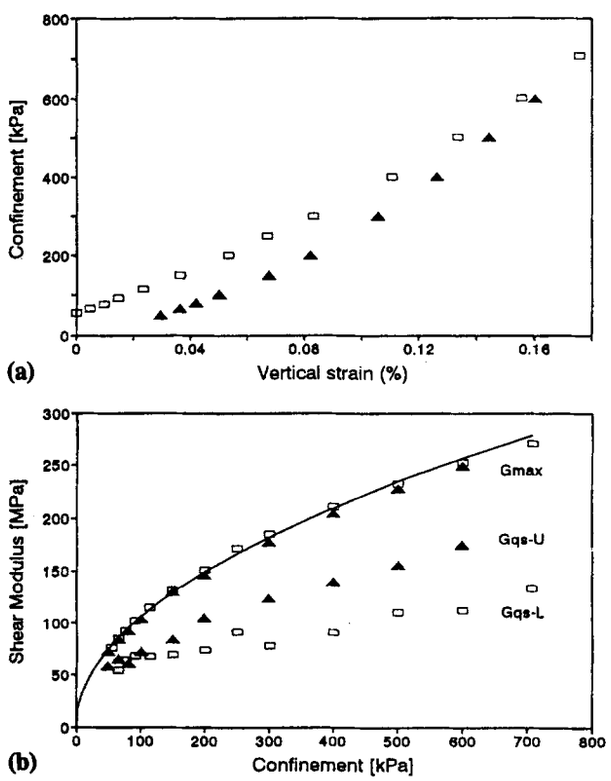

FIG. 8. Uniform Sand Subjected to Isotropic Loading: (a) Stress-Strain Curve; (b) Shear Modulus G_{max} and Quasistatic Modulus G_{qs} versus Confinement

FINAL COMMENTS AND CONCLUSIONS

The effect of contact behavior on wave velocity and attenuation was studied with four particulate materials: steel spheres to model elastic deformations, lead shot to assess viscoplastic response and rheological effects, silica-kaolinite pellets to evaluate the consequences of brittle contact behavior, and data for quartz sand were presented for comparison.

In agreement with theoretical predictions, velocity-stress and damping-stress data approach power relations. Velocity-strain and damping-strain plots for all tested materials also show a general power trend; V-ε and D-ε plots highlight differences between loading and unloading.

Table 2 presents a summary of regression parameters obtained from the fitting of velocity-stress and damping-stress data. Emphasis is placed on the dimensionless exponents $b/2$ and κ, which capture the nature of contacts. To a first approximation, dimensional constants are affected by material parameters, as indicated in (7), (10), and (14).

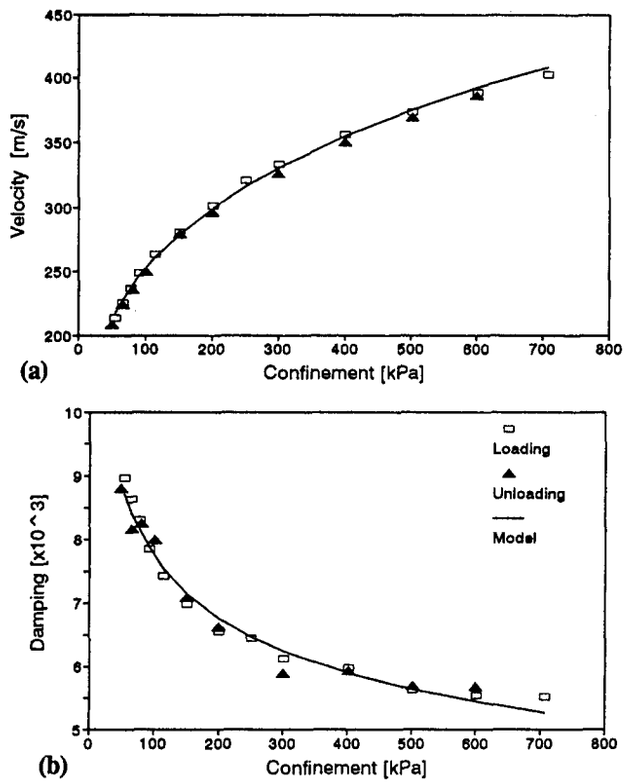

FIG. 9. Uniform Sand Subjected to Isotropic Loading: (a) Velocity versus Confinement; (b) Damping versus Confinement

TABLE 2. Summary of Test Results

Parameter (1)	Steel spheres (2)	Lead shot (3)	SF-K pellets (4)	Uniform sand (5)
$b/2$—loading	0.14	0.24–0.25	0.33–0.25	0.25
$b/2$—unloading	0.15	0.04	0.15	0.25
κ—loading	−0.40	−0.30	−0.15	−0.20
κ—unloading	−0.45	−0.32	−0.11	−0.20
Velocity range (m/s)	220–320	130–240	150–300	200–400
Damping range ($\times 10^{-3}$)	15–45	8–18	13–21	5.5–9.0
Pressure range (kPa)	35–250	70–600	25–500	50–700
Log (shear strain)	−5.5–−5.0	−5.9–5.65	−5.1–−4.7	−5.5–5.0
Maximum axial strain (%)	0.025	1.04	8.8	0.18
Residual strain (%)	0.005	1.00	8.5	0.03

Note: Elastic sphere contact (Hertz) $b/2 = 1/6$; elastic cone-plane contact $b/2 = 1/4$; plastic sphere contact $b/2 = 1/4$; and hysteretic loss (Mindlin) $\kappa = -2/3$.

All measured velocity-stress exponents were $b/2 > \approx 1/6$, which is the theoretical value for spherical contacts. High-tolerance steel spheres approximated this value. Contact crushing showed the highest exponent. Theoretical analyses confirmed that several phenomena conduce to a velocity-stress exponent $b/2 = 0.25$: buckling of particle chains and increase in coordination number, and elastoplastic behavior and cone-plane contacts.

Loading and unloading data for viscoplastic lead shot emphasized that contact deformation is the governing parameter for low-strain stiffness, regardless whether the causing mechanism was elastic deformation, creep, or yield. Thus, velocity-strain relations based on elastic Hertzian behavior [(8)] can be generalized to predict the low-strain stiffness of more complex elastoviscoplastic materials. The measured velocity-stress exponent for lead shot was remarkably close to the value predicted by this approach for a SC array with yielding contacts ($b/2 = 1/4$).

Preloading affects wave velocity in as much as it causes permanent changes in contact geometry or fabric. In general, the consequences of preloading are more pronounced in the midstrain modulus G_{qs}. This highlights that G_{max} is a measurement of *state* while the quasistatic modulus G_{qs} is a measurement of *change in state*. The analysis of soil data presented in this publication and other similar data sets available in our laboratory shows that the exponent $b/2$ tends to be the same or lower during unloading than during loading, particularly in loose soils. Table 2 shows that this situation also develops when contacts yield or break.

In the case of damping, all measured damping-stress exponents κ were between $\kappa = -0.45$ for steel and $\kappa = -0.11$ for the brittle pellets, while the theoretical value for frictional Mindlin contacts is $\kappa = -2/3$. This does not necessarily discard frictional loss as an energy-dissipation mechanism; the exponent κ also reflects the changes that occur in the material between successive measurements. However, the authors tested soils at constant stress and fabric but at varying excitation strain, and showed that frictional loss could not be justified as a sole loss mechanism at very low strains $\gamma < 10^{-7}$ (Santamarina and Cascante, in press, 1996).

Surface slippage could occur for steel spheres and lead shot, since the relative displacement between particles is around 130–300 Å for shear strains of $\gamma = 10^{-5}$ and particle diameters of 1.3–3 mm. In the case of visco plastic lead shot, damping increased during unloading in response to the decrease in contact forces, independently of the permanently flattened contact area. This is in agreement with Amonton's laws of friction.

Lead shot permits studying in short time the possible long-term diagenetic consequences in soils. Damping showed higher sensitivity than velocity to stress and time, and while wave velocity changed little during unloading, damping remained sensitive to contact forces and time effects. These results confirm that attenuation information is complimentary to velocity information in inversion problems of the state of stress.

Sustained loading seems to be more important than preloading in the case of damping. It is hypothesized that time and pressure influence the displacement of adsorbed layers and the formation of interparticle bonds (recall the sudden increase in damping in lead shot upon the application of a load increment). These effects do not seem to contribute to low-strain stiffness. It follows that the increase in stiffness with cementation (e.g., sometimes observed in marine environments) must result from an increase in the region of interparticle contact.

ACKNOWLEDGMENTS

Support for this research was provided by the Natural Sciences and Engineering Research Council of Canada (NSERC) and the University of Waterloo ID-Program. The writers are thankful to J. Wynnyckyj for his guidance in the preparation of pellets.

APPENDIX. REFERENCES

Acar, Y. B., and El-Tahir, E. A. (1986). "Low strain dynamic properties of artificially cemented sand." *J. Geotech. Engrg.*, ASCE, 112(11), 1001–1015.

Chang, C. S., Misra, A., and Sundaram, S. S. (1991). "Properties of granular packings under low amplitude cyclic loading." *Soil Dynamics and Earthquake Engrg.*, 10(4), 201–211.

Deresiewicz, H. (1973). "Bodies in contact with applications to granular media." *R. D. Mindlin and Applied Mechanics*, G. Herrmann, ed., Pergamon Press, New York, N.Y., 105–145.

Duffy, J., and Mindlin, R. D. (1957). "Stress-strain relations of a granular medium." *J. Appl. Mech.*, 24(4), 585–593.

Feda, J. (1992). "Creep of soils and related phenomena." Developments in Geotechnical Engineering, 68, Elsevier-Academia, Amsterdam, The Netherlands.

Field, W. G. (1963). "Towards the statistical definition of granular mass." *Proc., 4th Australian and New Zeland Conf. on Soil Mech.*, Instn. of Engrs., Australia, 143–148.

Goddard, J. D. (1990). "Nonlinear elasticity and pressure-dependent wave speeds in granular media." *Proc., Royal Society of London*, London, England, Vol. 430, 105–131.

Hardin, B. O., and Black, W. L. (1966). "Sand stiffness under various triaxial stresses." *J. Soil Mech. and Found. Engrg.*, ASCE, 92(2), 27–42.

Hardin, B. O., and Drnevich, V. P. (1972). "Shear modulus and damping in soils: Measurements and parameter effects." *J. Soil Mech. and Found. Engrg.*, ASCE, 98(6), 603–624.

Hardin, B. O., and Richart, Jr., F. E. (1963). "Elastic wave velocities in granular soils." *J. Soil Mech. and Found. Div.*, ASCE, 89(1), 33–63.

Ishihara, K. (1986). "Evaluation of soil properties for use in earthquake response analysis." *Geomechanical Modelling in Engineering Practice*, Dungar and J. A. Studer, eds., A. A. Balkema Publishers, Rotterdam, The Netherlands.

Lee, E. H., and Radok, J. R. M. (1960). "The contact problem for viscoelastic bodies." *Trans. of the ASME J. Appl. Mech.*, 27(9), 438–444.

Petrakis, E., and Dobry, R. (1987). "Micromechanical modeling of granular soil at small strain by arrays of elastic spheres." *Rep. CE-87-02*, Dept. of Civ. Engrg., Rensselaer Polytechnic Inst., Troy, N.Y.

Richart, Jr., F. E., Hall, J. R., and Woods, R. D. (1970). *Vibration of soils and foundations*. Prentice Hall, Inc., Englewood Cliffs, N.J.

Rothenburg, L., and Bathurst, R. J. (1989). "Analytical study of induced anisotropy in idealized granular material." *Geotechnique*, London England, 39(4), 601–614.

Santamarina, J. C., and Cascante, G. (1996). "Stress anisotropy and wave propagation—A micromechanical view." *Canadian Geotechnical Journal*, Vol. 33, October.

Saxena, S. K., Avramidis, A. S., and Reddy K. R. (1988). "Dynamic moduli and damping ratios for cemented sands at low strains." *Can. Geotech. J.*, 25(2), 353–368.

Scott, G. D., Charlesworth, A. M., and Mak, M. K. (1964). "On the random packing of spheres." *J. Chem. Phys.*, 40(2), 611–612.

Singh, A., and Mitchell, J. K. (1968). "General stress-strain-time function for soils." *J. Soil Mech. and Found. Engrg. Div.*, ASCE, 94(1), 21–46.

Smith, W. O., Foote, P. D., and Busang P. F. (1929). "Packing of homogeneous spheres." *Phys. Rev.*, 34(9), 1271–1274.

Stokoe, K. H., Lee, S. H., and Knox, D. P. (1985). "Shear moduli measurements under true triaxial stresses." *Proc., Adv. in the Art of Testing Soils Under Cyclic Conditions*, Geotech. Engrg. Div., ASCE, New York, N.Y., 166–185.